P2.13 FINDING BOUNDARY LAYER TOP FOR THE STABLE LAYER: APPLICATION OF A HAAR WAVELET COVARIANCE TRANSFORM TO LIDAR OBSERVATIONS

Ian M. Brooks*
Scripps Institution of Oceanography, La Jolla, California

1. INTRODUCTION

Direct measurement of the entrainment rate across the atmospheric boundary layer (BL) inversion is not possible; it must be estimated indirectly from other measurements (Lenschow et al 1999). In contrast the structure of the entrainment zone is relatively easy to characterize using remote sensing techniques such as lidar (Boers et al. 1984; Melfi et al. 1985; Crum et al. 1987; Flamant et al. 1997). Lidar reveals the interface between the BL and the free troposphere by the change in backscattered light between the two layers – usually the BL has a significantly higher concentration of aerosol than the air above and thus produces a greater backscatter. Swelling of the aerosol due to the high relative humidity near BL top also contributes to a greater backscatter. Cloud is even more easily identified since it produces a very high backscatter, often saturating the detector.

Identification of BL top from the lidar backscatter signal has been achieved by a variety of means: an entirely subjective identification by eye (Boers et al. 1984), a threshold value above the background signal (Melfi et al. 1985), and most commonly a minimum in the vertical gradient (Flamant et al. 1997). Recently a new approach utilizing wavelets has been used with considerable success (Russell et al. 1998; Cohn and Angevine 2000, Davis et al. 2000).

2. WAVELET ALGORITHM

The wavelet algorithm used here follows that described by Davis et al. (2000). A Haar wavelet basis function, h, is defined as

$$h\left(\frac{z-b}{a}\right)=\begin{cases}+1 & : \quad b-a/2 \le z \le b \\ -1 & : \quad b \le z \le b+a/2 \\ 0 & : \quad elsewhere\end{cases} \qquad (1)$$

Where z is altitude, b is the location at which the Haar function is centered (the *translation* of the function), and a is the wavelet dilation. Gamage and Hagelberg (1993) define a covariance transform

$$W_f(a,b)=\frac{1}{a}\int_{z_b}^{z_t} f(z)\,h\left(\frac{z-b}{a}\right)dz \qquad (2)$$

Where z_b and z_t define the bottom and top of the backscatter profile, and $f(z)$ is the backscatter signal. A maxima in W_f identifies a step in $f(z)$ at an altitude $z=b$, and with a coherent vertical scale of a (Figure 1). The key to effectively identifying the boundary of interest is in the selection of an appropriate value for a. Davis et al. (2000) demonstrate that for the simple case where the mean backscatter is near-constant both within and above the BL the choice of a is not crucial provided it is large enough to distinguish the inversion from small-scale variability in the signal. Where the backscatter departs from this ideal because of vertical gradients or large-scale structure in the signal – not uncommon in stably stratified layers – the problem becomes more complex and our choice of a may bias the value obtained for BL top.

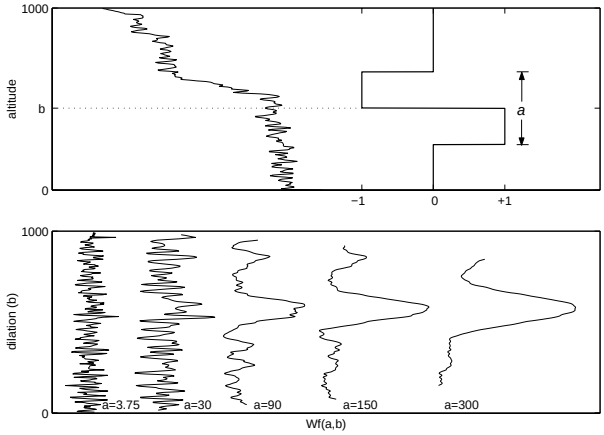

Figure 1. An example of a lidar backscatter profile and haar wavelet (upper panel) and the resulting covariance transform at various dilations (lower panel).

Note that the useful values of a and b are constrained by the length of the profile. If b is closer than $a/2$ to an end of the profile, then the convolution is undefined where part of the wavelet extends beyond the data. We thus limit the translation to values for which the convolution is defined. Also, if $a/2$ is greater than the distance from the inversion to the end of the profile, then the limit imposed on the translation prevents the wavelet from coinciding with the inversion, which can thus not be identified.

3. THE EFFECT OF VERTICAL GRADIENTS

There are three distinct regions where different mean gradients in backscatter may be found: within the BL, above the BL, and across an inversion layer. Since the

* *Corresponding Author address*: Ian M. Brooks, Integrative Oceanography Division, SIO-UCSD, 9500 Gilman Drive, La Jolla, CA. 92093-0209; email ibrooks@ucsd.edu

problem is essentially symmetric about the inversion (it makes little difference mathematically if we work down from the top of the profile, or up from the bottom) we will assume the BL backscatter to be constant in the conceptual cases below, and deal with gradients only in and above the inversion.

We consider first the effect of the gradient across an inversion of finite thickness. Figure 2 shows the idealized backscatter profile and the value of the wavelet translation $b(W_{f\max})$ as a function of dilation, a.

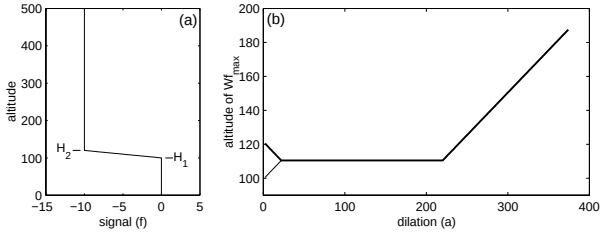

Figure 2. (a) An idealized profile with constant backscatter above and below the inversion, and a gradient $df/dz=G_1$ across the inversion. (b) The translation at which W_f has its maximum plotted against dilation. For small values of a the location of $W_{f\max}$ has multiple values – the upper and lower limits are shown.

For dilations less than the inversion depth, $\Delta H=H_2-H_1$, the wavelet fits entirely within the inversion layer and W_f has a constant (and maximum) value; thus the altitude of the maximum is not unique; the upper and lower limits are shown on the figure. For the smallest possible dilation – a 2 point difference – these limits are the bottom and top of the inversion layer, H_1 and H_2. As the dilation increases the limits converge towards the midpoint of the inversion layer. For $\Delta H<a<(2H_1+\Delta H)$ a single, constant, value of $b(W_{f\max})=H_1+\Delta H/2$ is found. For $a>(2H_1+\Delta H)$ the dilation is greater than the mixed layer depth and $b(W_{f\max})=a/2$.

Now consider the case where there are gradients both across and above the inversion layer, G_1 and G_2 respectively (figure 3).

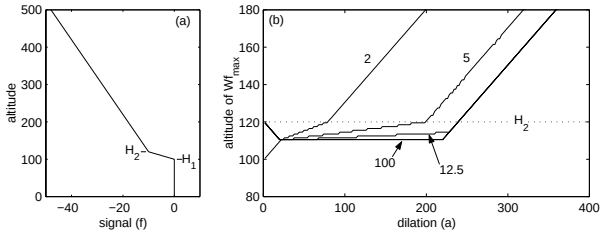

Figure 3. (a) Idealized profile with constant backscatter below the inversion, and gradients $df/dz=G_1$ across the inversion, and G_2 above the inversion. (b) The translation at which W_f is a maximum plotted against dilation for the values of G_1/G_2 noted against each line.

Three regions can be identified from figure 3. For $a<\Delta H$ a range of values within the inversion layer are found, as for the previous case. For a given value of G_1/G_2 there is a threshold dilation at which $W_{f\max}$ occurs at the top of the inversion; if a increases beyond this, then $b(W_{f\max})$ increases linearly with $a/2$. For smaller values of the dilation $b(W_{f\max})$ increases with a at a rate determined is dependent on the ratio G_1/G_2 as illustrated by the four cases shown. For our idealized case we can find an exact analytical expression for $W_f(a,b)$; the behavior of $b(W_{f\max})$ in this last region can then be found by maximizing this function. In this manner we find that for $a>\Delta H$

$$b(W_{f\max}) = H_1 + \frac{\left(\frac{G_1}{G_2}\Delta H + \frac{a}{2}\right)}{\left(2\frac{G_1}{G_2} - 1\right)} \qquad (3)$$

This expression is valid up to a limiting dilation at which $b(W_{f\max})$ starts to increase as a function of $a/2$; there are two separate limits: the first applies for large values of G_1/G_2 where (3) intercepts the line $b=a/2$, this gives

$$a_1 = H_1 + \frac{\left(\frac{G_1}{G_2}H_2\right)}{\left(\frac{G_1}{G_2} - 1\right)} \qquad (4)$$

The second applies for smaller values of G_1/G_2 and occurs when (3) intercepts the line $b=H_2$; this gives

$$a_2 = 2\Delta H\left(\frac{G_1}{G_2} - 1\right) \qquad (5)$$

For dilations greater than this we will get

$$b(W_{f\max}) = H_2 + \left(\frac{a}{2} - \Delta H\left(\frac{G_1}{G_2} - 1\right)\right) \qquad (6)$$

The limiting value of G_1/G_2 at which the transition between the limiting dilations in (4) and (5) occurs can be found by substituting $a=2H_2$ in to either expression, and gives

$$\frac{G_1}{G_2} = \frac{H_2}{\Delta H} + 1 \qquad (7)$$

a_1 or a_2 gives the upper limit to the useful range of dilations for a given environment. It is obvious from figure 3 that over most of this range $W_{f\max}$ will occur between the midpoint and top of the inversion. The ideal choice of dilation is $a>\Delta H$, which would identify the midpoint of the inversion regardless of the gradients within or above it.

The discussion above relates to a highly idealized backscatter profile and its application might appear problematical since Identification of the limiting dilations requires a priori knowledge of the very terms we are attempting to measure. Also, real lidar profiles exhibit significant small-scale variability arising from structure in the boundary layer caused by mixing and differential advection of air masses, this structure can change

noticeably over relatively small horizonatal distances. The large-scale structure, however, tends to change little over relatively large distances. We might thus consider the idealized case as the ensemble average of a set of backscatter profiles; individual estimates of $b(W_{f\max})$ would then be expected to scatter about the analytical expressions. It is also apparent from that, except for $a<\Delta H$, this approach will only identify a point between the midpoint and the top of the inversion. Only with the smallest dilation possible is the bottom of the inversion (the top of the mixed layer) identified; this presents a problem since figure 1 shows that the smallest dilations reveal only the small-scale variability and noise in the signal.

4. APPLICATION TO REAL DATA

We now examine the application of this approach to an observed backscatter profile – the same profile shown in figure 1, but truncated to a maximum altitude of 850 m to remove the additional complication of another step in the signal (Figure 4); the limits of the range of BL top

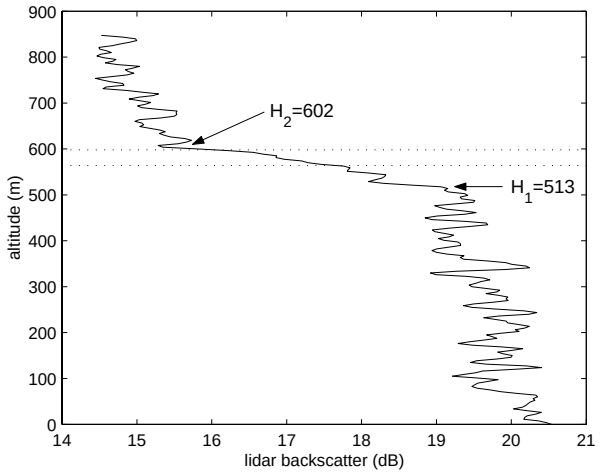

Figure 4. Lidar backscatter profile. The top and bottom of the inversion have been estimated, along with the gradient across the inversion (G_1=0.04) and above the inversion (G_2=0.0044). The upper and lower limits of the BL top identified by the wavelet algorithm are indicated by dotted lines.

values identified are shown as dotted lines – note that this encompasses the upper half of the inversion layer only. The vertical resolution of the lidar profile is 3.75 m; the wavelet algorithm is implemented with dilation increments of 7 m and centered between lidar samples. Figure 5 shows the individual values plotted against wavelet dilation; the theoretical value of $b(W_{f\max})$ given by (3) is plotted as a dotted line – the observed values fit this line well over it's range of validity (approximately 100-500 m). For $a<\Delta H$ (89 m) only a single value of $b(W_{f\max})$ is found rather than the multiple values found for the idealized case; this is expected since the constant value of W_f occurs only for a uniform gradient – here, small-scale variations in backscatter introduce variability into W_f. The points scatter around the upper

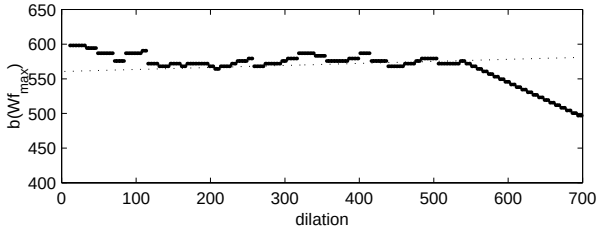

Figure 5. $b(W_{f\max})$ plotted against dilation, a, (the two smallest values of a (3.75 and 7 m), gave b=129 m and are not shown). The dotted line is given by the analytical expression (3) and H_1, H_2, G_1, and G_2 estimated from figure 4.

limit of the idealized range due to the greater gradient in backscatter across the upper inversion. At the two smallest dilations (7.5 and 15 m) the inversion is indistinguishable from the small-scale structure in the backscatter and $b(W_{f\max})$ occurred at ~100 m (not shown).

For large dilations, $b(W_{f\max})$ decreases with a uniform gradient of -0.5. This results from the wavelet running up against the top of the profile – since the inversion is closer to the top of the profile than the surface, this limit on useful dilation is inverted with respect to the idealized example above. Note that the point at $b(W_{f\max})$ starts to decrease is twice the distance from the inversion top to the top of the profile.

Figure 6 shows profiles of W_f for dilations of 45, 90, and 300 m, with the locations of $b(W_{f\max})$ marked. Of particular interest is the case with a=45 m – approximately half the thickness of the inversion layer. Here $b(W_{f\max})$ is well defined and identifies a point very close to the top of the inversion. A second peak in W_f, only slightly smaller, is located at 518 m, within one sample of the location of the bottom of the inversion layer. This provides us with a potential means of identifying both the upper and lower limits of the inversion layer.

5. SUMMARY

An analytical treatment of the application of a Haar wavelet covariance algorithm to an idealized lidar profile with vertical gradients across and above the inversion

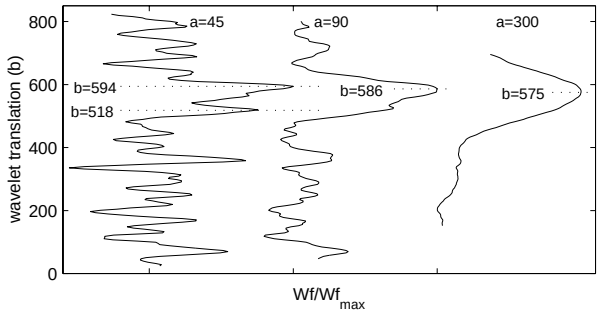

Figure 6. Profiles of W_f normalised by their maximum values for dilations of 45, 90, and 300 m. The altitude of each maximum is marked. Ticks on the abscissa indicate W_f =0 for each profile

layer shows that the value of $b(W_{f\max})$ is dependent upon the wavelet dilation chosen, the ratio of the gradients, and the depth of the inversion layer. In general we expect to identify a point between the mid-point and top of the inversion; the bottom of the inversion is identified only with the smallest possible dilation – this is impractical for real data due to the effects of small-scale structure in the signal. Application to an observed lidar profile demonstrates that small-scale structure in the backscatter profile introduces scatter around the results predicted by the idealized analysis. Depending upon the details of the structure in and around the inversion, a mean bias towards higher or lower values may also be introduced. Examination of W_f profiles for dilations close to half the depth of the inversion layer indicate that the two largest peaks identify the upper and lower limits of the inversion. We note that a traditional gradient approach (eg Flamant et al, 1997) would allow an estimate only of the mid-point of the inversion to be made.

In order to make best use of this approach we require a priori knowledge of the very quantities we are attempting to measure. We might estimate approximate values from a visual inspection of the data and apply these as 'first guess' values to the processing of data obtained under relatively uniform conditions. This is a less than ideal approach, and may not be practical where the mean BL depth, inversion thickness, or both change significantly, for example in cases where strong convective plumes are present. Fully automated algorithms will require more sophisticated processing of the data. Currently under evaluation are a number of possible approaches:

- Filtering of individual profiles to remove the smallest-scale structures, allowing initial estimates of H_1, H_2 and mean gradients to be made; these can be used to chose a dilation to use to the unfiltered profile.
- Examination of W_f profiles for multiple dilations; correlation of the locations of two most significant peaks may be used to identify probable values of H_1 and H_2 and thus the appropriate dilation to use.
- Examination of the statistics of $b(W_{f\max})$ for the full range of dilations to estimate BL depth and inversion thickness.

These results also provide some guidance for flight planning when taking lidar observations with the intention of examining the inversion structure; in particular the ideal flight level is approximately double the mean BL depth, so as to ensure the widest possible range of dilations can be used. Flying too close to the BL top will restrict the dilations that can be used to relatively small values.

Acknowledgements. This work was supported by the National Science Foundation: grant ATM-0100685, and the Office of Naval Research: grant N00014-01-1-0258.

REFERENCES

Boers, R., E. W. Eloranta, and R. L. Coulter, 1984: Lidar observations of mixed layer dynamics: tests of parameterized entrainment models of mixed layer growth rate. *J. Climate Appl. Meteorol.*, **23**, 247-266.

Cohn, S. A., and W. M. Angevine, 2000: Boundary-layer height and entrainment zone thickness measured by lidars and wind profiling radars. *J. Appl. Meteorol.*, **39**, 1233-1247.

Crum, T. D., R. B. Stull, and E. W. Eloranta, 1987: Coincident lidar and aircraft observations of entrainment into thermals and mixed layers. *J. Climate Appl. Meteorol.* **26**, 774-788.

Davis, K. J., N. Gamage, C. R. Hagelberg, C. Kiemle, D. H. Lenschow, and P. P. Sullivan, 2000: An objective method for deriving atmospheric structure from airborne lidar observations. *J. Atmos. Oceanic. Technol.*, **17**, 1455-1468.

Flamant, C., J. Pelon, P. H. Flamant, P. Durand, 1997: Lidar determination of the entrainment zone thickness at the top of the unstable marine atmospheric boundary layer. *Bound.-Layer Meteorol.*, **83**, 247-284.

Gamage, N., and C. Hagelberg, 1993: Detection and analysis of microfronts and associated coherent events using localized transforms. *J. Atmos. Sci.*, **50**, 750-756.

Lenschow, D. H., P. B. Krummel, and S. T. Siems, 1999: Measuring entrainment, divergence, and vorticity on the mesoscale from aircraft. *J. Atmos. Oceanic. Tech.*, **16**, 1384-1400.

Melfi, S. H., J. D. Sphinhirne, S. H. Chou, and S. P. Palm, 1985: Lidar observations of the vertically organized convection in the planetary boundary layer over the ocean. *J. climate Appl. Meteorol.*, **24**, 806-821.

Russell, L. M., D. H. Lenschow, K. K. Laursen, P. B. Krummel, S. T. Siems, A. R. Bandy, D. C. Thompson, and T. S. Yates, 1998: Bidirectional mixing in an ACE 1 marine boundary layer overlain by a second turbulent layer. *J. Geophys. Res.*, **103**, 16411-16432.